Polymers **2014**, *6*, 2435-2450; doi:10.3390/polym6092435

OPEN ACCESS

polymers

ISSN 2073-4360

www.mdpi.com/journal/polymers

Article

Structural, Optical and Electrical Properties of PVA/PANI/Nickel Nanocomposites Synthesized by Gamma Radiolytic Method

Abdo Mohd Meftah [1], Elham Gharibshahi [2], Nayereh Soltani [2], W. Mahmoud Mat Yunus [2] and Elias Saion [2,*]

[1] Department of Physics, Faculty of Applied Sciences, Thamar University, Dhamar, P.O. Box 47246, Yemen; E-Mail: benmaftah@yahoo.com

[2] Department of Physics, Faculty of Science, Universiti Putra Malaysia, Serdang, Selangor 43400, Malaysia; E-Mails: ehlamgs2002@yahoo.com (E.G.); nayereh.soltani@gmail.com (N.S.); mahmood@science.upm.edu.my (W.M.M.Y.)

* Author to whom correspondence should be addressed; E-Mail: emansaion@gmail.com; Tel.: +60-389-466-646; Fax: +60-389-454-454.

Received: 21 February 2014; in revised form: 2 June 2014 / Accepted: 21 July 2014 / Published: 24 September 2014

Abstract: This article reports a simultaneous synthesis of polyaniline (PANI) and nickel (Ni) nanoparticles embedded in polyvinyl alcohol (PVA) film matrix by gamma radiolytic method. The mechanism of formation of PANI and Ni nanoparticles were proposed via oxidation of aniline and reduction of Ni ions, respectively. The effects of dose and Ni ions concentration on structural, optical, and electrical properties of the final PVA/PANI/Ni nanocomposites film were carefully examined. The structural and morphological studies show the presence of PANI with irregular granular microstructure and Ni nanoparticles with spherical shape and diameter less than 60 nm. The average particle size of Ni nanoparticles decreased with increasing dose and decreasing of precursor concentration due to increase of nucleation process over aggregation process during gamma irradiation. The optical absorption spectra showed that the absorption peak of Ni nanoparticles at about 390 nm shifted to lower wavelength and the absorbance increased with increasing dose. The formation of PANI was also revealed at 730 nm absorption peak with the absorbance increasing by the increase of dose. The electrical conductivity increased with increasing of dose and chlorine concentration due to number of polarons formation increases in the PVA/PANI/Ni nanocomposites.

Keywords: polyaniline (PANI); nickel (Ni) nanoparticles; polyvinyl alcohol (PVA); gamma radiolytic method; absorbed dose

1. Introduction

Conducting polymers are conjugated chain of organic compounds that display high electrical conductivity similar to metals because of the present of large carrier concentrations of extended π-electrons, known as polarons, which allow charge mobility along the backbone of the polymer chain. Their electrical conductivities are comparable with metals but polymers have many advantages, such as being light-weight, resistance to corrosion, flexibility, and low cost. Conducting polymers are finding numerous applications in television sets, cellular telephones, displays, light emitting diodes, solar cells, batteries, actuators, sensors, electromagnetic shielding, and microelectronic devices [1–3]. Amongst the family of conducting polymers, polyaniline (PANI) has been of particular interest due to its controllable electrical conductivity, high absorption coefficients in the visible light, interesting redox properties, chemical stability, relatively high conductivity, easy polymerization, and low cost of monomer [1–6]. The synthesis of PANI has been mostly accomplished by oxidation of aniline through chemical [7], electrochemical [8], photolysis [9] or radiation [1,10] methods.

PANI combined with inorganic nanoparticles such as silver [5,9], gold [11], Copper [12], CeO_2 [3] and TiO_2 [13] to form PANI/metal nanoparticle nanocomposites in order to improve physical, mechanical, and electrical properties. The obtained nanocomposites have characteristic advantages between their single component counterparts [2,3] and can have potential applications in new device. In particular, transition metal nanoparticles dispersed within a polymer matrix offer attractive routes for combining properties stemming from metal nanoparticles and from that of polymers [14]. The incorporation of metal nanoparticles could effectively improve the optical and dielectric properties of the PANI composites. The nanoparticles could act as conductive junctions between the PANI chains that resulted in an increase of the electrical conductivity of the composites [2]. The composites of PANI with magnetic metal nanoparticles are also promising candidates, based on the fact that the small sized particles enhance the physical properties while the conducting polymer matrix present electrical host-guest interaction to occur in a new magneto-electric phenomenon at the same time, allowing coupling between magnetic and electric properties for future devices.

Among metal nanoparticles used, nickel (Ni) nanoparticles are of great interest in the modern materials world due to special electronic, optical, and magnetic properties [15,16] and its wide variety of applications in catalysis [17], conducting inks, multi-layered ceramic capacitors, microelectronics, thick-film electrode material, and solar-cells [18]. Ni nanoparticles can be prepared through many methods, such as chemical-electrochemical methods [19], laser ablation of solids in organic solution [20], thermal decomposition [21,22], microwave assisted [23], conventional polyol process [24], low pressure spray-pyrolysis method [25], gas phase process [26], sonochemical [27,28], and microemulsions synthesis [29] with various reducing agents. There are also a number of reports on the synthesis of Ni nanoparticles embedded in PANI using direct current magnetron sputtering [30], chemical [14,31], and eltrochemical [32,33] methods. However, fabrication of PANI/Ni nanocomposite films without

using of toxic chemical agents still remains highly challenging. This challenge may be met meaningfully by employing simple and mild γ irradiation technique which has a capability to produce conducting polymer and metal nanoparticle components at the same time without using any chemical agents.

In this study, PANI and Ni nanoparticles embedded in polyvinyl alcohol (PVA) film matrix were simultaneously prepared by gamma rays induced oxidation of aniline and reduction of Ni ions. The composites of PVA/PANI/Ni nanoparticles irradiated at different doses were extensively studied for their structural, optical, and electrical properties. The PVA/PANI/Ni nanocomposites film matrix could have underpinning behaviors between electrical property of PANI and optoelectronic property of metal or semiconductor nanoparticles for a new device.

2. Experimental Section

Poly(vinyl alcohol) (PVA) (M_W = 85,000 g/mol) supplied by Sigma Aldrich (St. Louis, MO, USA), aniline monomer (M_W = 93.13 g/mol) by Fulka Chemie (Buchs, Switzerland) and nickel chloride ($NiCl_2 \cdot 6H_2O$, M_W = 237.7 g/mol) by Hamburg Chemical GmbH (Hamburg, Germany) were used to synthesize PVA/PANI/Ni nancomposites film matrix. The PVA bulk solution was first prepared by dissolving 30 g of PVA powder in 600 mL distilled water at 90 °C andcontinuous stirring for 3 h before left to cool at room temperature. Subsequently, 4 g of aniline monomer was added into 100 mL PVA solution under stirring. Next, different nickel chloride concentrations from 10 to 22.5 wt% were added to the solution and stirred continuously for 6 h. Each blend solution was poured in the Petri dish on flat surface and dried in ambient temperature for several days until the free standing film can be peeled off and cut into several pieces. The average thickness of the standing films was about 1.96 mm. The samples were irradiated with 1.25 MeV gamma radiation from ^{60}Co source (Gammacell model Excel 220 S. N. 117 R) in the dose range of 0–50 kGy.

After irradiation, the samples underwent characterization using X-ray diffraction (XRD) of 7602EA model (PANalytical B.V., Almelo, The Netherlands) with copper *K*α radiation at 1.5418 Å wavelengths, scanning electron microscopy (SEM) model Philips XL30 (FEI Company, Eindhoven, The Netherlands) at an accelerating voltage of 20 kV, atomic force microscopy (AFM) of Digital Instruments Dimension 3100 (Veeco Instruments Inc., Camarillo, CA, USA), UV-visible spectrophotometer of SHIMADZU 1650 PC (SHIMADZU Corporation, Tokyo, Japan), transmission electron microscopy (TEM) of Hitachi H-7100 (Hitachi Ltd., Tokyo, Japan) at an accelerating voltage of 200 kV, and conductivity measurement with Precision LCR impedance meter of HP 4284A (Hewlett-Packard Japan Ltd., Tokyo, Japan).

3. Results and Discussion

3.1. Formation of Polyaniline (PANI) and Nickel (Ni) Nanoparticles

1.25 MeV gamma rays interact with the hydrated film samples by photoelectric absorption, Compton scattering, and pair production. These results in the formation of secondary electrons, mainly by Compton scattering that induce among others hydrated electron (e^-_{aq}), hydroxyl radical (OH·), and hydrogen radical (H·) by radiolysis of water according to Equation (1) [34]:

$$H_2O\cdot \xrightarrow{\gamma\text{-rays}} e^-_{aq},\ H^+,\ H_3O^-,\ H\cdot,\ OH\cdot,\ H_2,\ H_2O_2 \text{ (radiolysis of water)} \quad (1)$$

The formation of Ni nanoparticles can be described by the following reactions [34]:

$$NiCl_2 \rightarrow Ni^{2+} + 2Cl^{-}(\text{ions dissociation}) \quad (2)$$

$$Ni^{2+} + 2e^{-}_{aq} \rightarrow Ni^{0} \text{ (first nucleation)} \quad (3)$$

$$Ni^{0} + Ni^{0} \rightarrow Ni^{0}_{2} \text{ (agglomeration)} \quad (4)$$

$$Ni^{0}_{m} + Ni^{0} \rightarrow Ni^{0}_{m+1} \text{ (agglomeration)} \quad (5)$$

In hydrated PVA films, nickel chloride dissociates into positive Ni^{2+} cations and negative $2Cl^{-}$ anions, Equation (2). The hydrated electrons reduce Ni^{+} into zero valent Ni atoms (Ni^{0}) by the nucleation process, Equation (3). A number of Ni^{0} atoms can agglomerate to form $Ni0_2$ or Ni^{0}_{m+1} nanoparticle, as shown in Equations (4) and (5), respectively.

The subsequent chemical effect of aniline monomer is that Cl^{-} anions can act as an oxidizing agent for doping "*in situ*" aniline monomer (C_6H_5NH), by polymerization of imines to an electrically conductive polyaniline (PANI) in the form of emeraldine salt (EB). In general, the conjugated PANI can exist in two different chemical structures depending on the degree of oxidation or protonation. The insulating emeraldine base consists of equal number of oxidized (imines) and reduced (amines) units. This structure is known as leucoemeraldine salt (LB). On the other hand, the conducting PANI is formed by protonation at imines (–N=) sites. In our case, Cl^{-} ions act as an oxidant to N^{+} sides and polymerized imines group into oxidized conjugated units of conducting PANI. The possible reaction mechanism for the formation of conducting PANI from gamma-radiation doping of aniline monomers by Cl^{-} anions may be written in the following form [1]:

$$2nC_6H_5NH + nNiCl_2 \cdot 6H_2O \xrightarrow{h\upsilon} n[C_6H_5NH] \cdot n[C_6H_5HN^{+} \cdot Cl^{-}] + nHCl + 6nH_2O + nNi^{+} \quad (6)$$

–(Polyaniline)–

The first term of Equation (6) represents the PANI chemical structure. The chemical structure of PVA matrix consists of C–C, C–H, and C–OH covalent bonds. The binding energy of C–C bond is much stronger than C–H and C–OH bonds and thus at doses below 50 kGy, the radiation effect on PVA is likely to cause some bonds breaking of C–H and C–OH [35] and they would not affect the formation of PANI or Ni nanoparticles.

3.2. Structural and Morphological Properties

3.2.1. X-ray Diffraction (XRD) Spectra

The X-ray diffraction (XRD) patterns of composite PVA/PANI/Ni nanoparticles are shown in Figure 1, where there are four Bragg's diffraction peaks appearing at 2θ values of 20°, 31.7°, 45.5° and 56.6°. A broad peak centered at 2θ = 20° corresponds to the PVA crystalline phase with the accepted monoclinic unit cell [36]. The strong diffraction peaks at 2θ values of 31.7°, 45.5° and 56.6° are associated respectively to (111), (200) and (222) crystalline plans of the face-centered cubic (FCC) structure of nickel nanoparticles. The intensity of these peaks increased with increasing of dose which is probably due to increase number of the Ni nanoparticles as confirmed by the optical study.

Figure 1. Typical X-ray diffraction (XRD) patterns of irradiated samples of 18.2 wt% metal precursor concentration at various doses up to 50 kG.

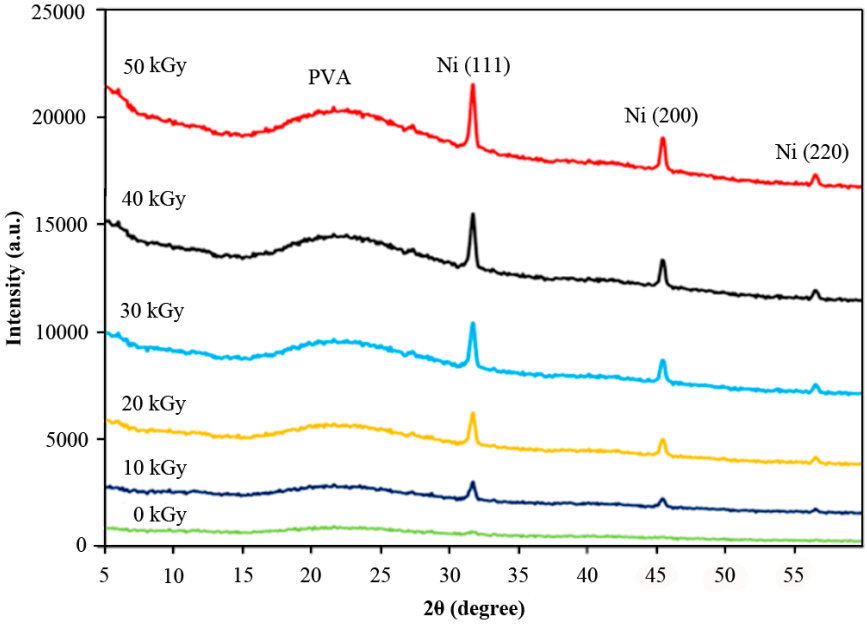

In order to further investigate the relationship between XRD pattern and particle size, the crystallite size of Ni nanoparticles was calculated from the major diffraction peak of the corresponding Ni, using the Debye–Scherer formula [37]:

$$D = k\lambda/\beta\cos\theta \quad (7)$$

where k is a constant, often taken as 0.9, λ is the wavelength of 5.9 keV Cu *K*α X-ray radiation (1.5418 Å), θ is the diffraction angle and β is the full width at half maximum (FWHM) of prominent intensity peak. The crystallite sizes of Ni nanoparticles were estimated using Debye–Scherrer formula through the preferred plan of (111). The variations of Ni particle size synthesized with different concentrations of $NiCl_2$ *versus* dose are shown in Figure 2. The particle size decreased exponentially with increasing of dose from 10 to 50 kGy. This finding of decreasing particle size of metal nanoparticles with increasing dose is in agreement with the studies carried out previously [38,39].

At low doses, the nucleation concentration, Ni^0, is considerably lower than the concentration of unreduced Ni^{2+} ions. Thus, more $Ni^0{}_m$ nanoparticles could be ionized by $Ni^{2+}{}_n$ ions to form larger $Ni^{2+}{}_{m+n}$ ions, Equation (8), and consequently reduced by hydrated electrons into larger $Ni^0{}_{m+n}$ nanoparticles, Equation (9). On the other hand, at higher doses, most of Ni^{2+} ions were consumed during nucleation processes. Hence, the nucleation concentration, Ni^0, is considerably higher than the unreduced Ni^{2+} ions. Since most of the $Ni^0{}_m$ nanoparticles were not ionized by $Ni^{2+}{}_n$ ions, therefore, the Ninanoparticles were smaller in size at higher doses [34]:

$$Ni^0{}_m + Ni^{2+}{}_n \rightarrow Ni^{2+}{}_{m+n} \text{ (second nucleation)} \quad (8)$$

$$Ni^{2+}{}_{m+n} + 2e^-_{aq} \rightarrow Ni^0{}_{m+n} \text{ (agglomeration)} \quad (9)$$

Figure 2. Average size of Ni nanoparticles *versus* dose for synthesized nanoparticles with different metal precursor concentrations.

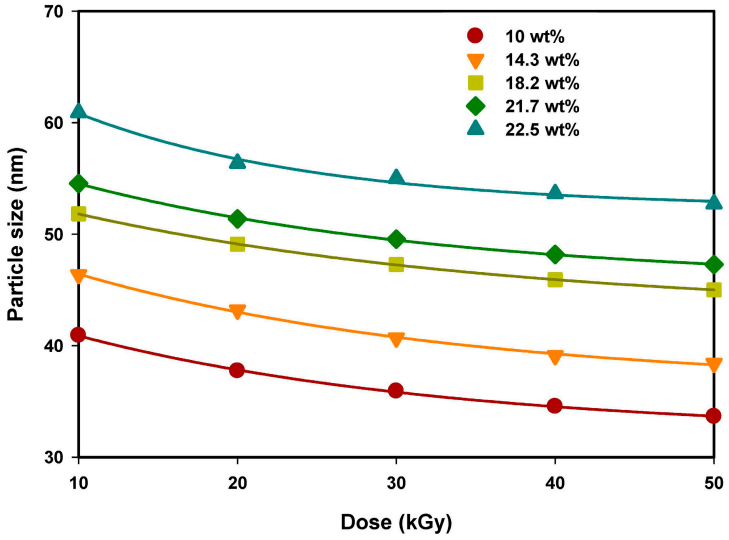

3.2.2. Transmission Electron Microscopy (TEM) Micrographs

Figure 3a shows typical TEM micrograph of composite PVA/PANI/Ni nanoparticles irradiated at 30 kGy dose showing the formation of PANI (light colour) and Ni nanoparticles (dark colour) embedded in PVA matrix. The Ni nanoparticles are almost spherical in shape. Figure 3b shows the particle density or size distribution histogram of Ni nanoparticles.

Figure 3. (**a**) TEM micrographs and (**b**) corresponding size distribution histogram with Gaussian fitting of Ni nanoparticles synthesized by γ-rays for 18.2 wt% metal precursor concentration stabilized in PVA and irradiated at 30 kGy.

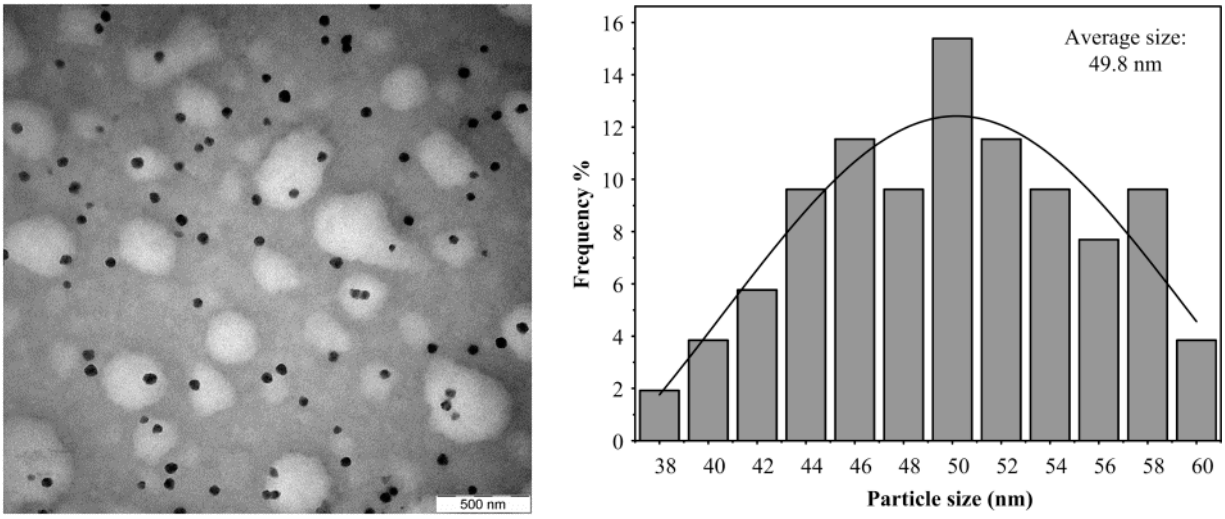

(**a**) (**b**)

3.2.3. Surface Morphology

The morphology of composites PVA/PANI/Ni nanoparticles were studied by scanning electron microscope (SEM) shown in Figure 4. The SEM micrograph reveals the formation of conducting

PANI nanostructures distributed almost uniformly on PVA matrix film. The granule shape was about 150–500 nm in diameter. This finding is in agreement with Yang and Chen [40] who reported irregular granular structure of chemically synthesized PANI containing transition metal ions of nickel and cobalt. This indicates that the complexion of transition metal ions to PANI greatly change the aggregation state of PANI molecular chains. There have been reported that the diameters of the PANI nanoparticles polymerized chemically with hydrochloric acid were about 100 to 150 nm for PVA/PANI nanocomposites [41] and 40 nm for PVP/PANI nanocomposites [42]. This suggests that the type of binder determined the diameter of spherical PANI.

Figure 4. SEM micrographs of PVA/PANI/Ni nanoparticles irradiated by 40 kGy ^{60}Co γ-rays for 18.2 wt% metal precursor concentration.

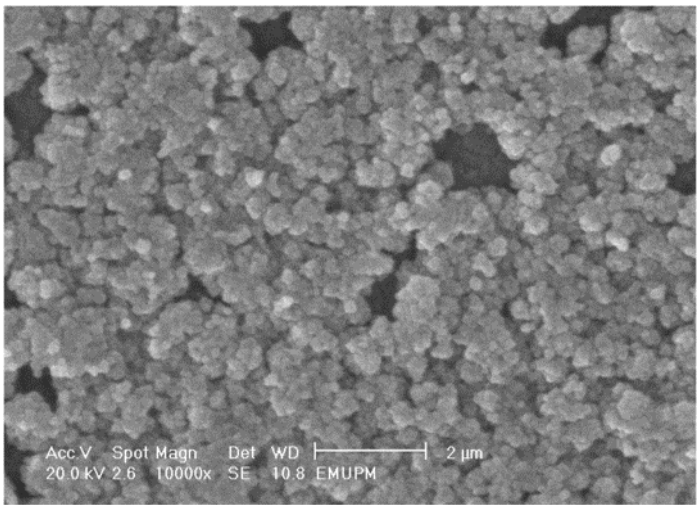

In principle we can use AFM images to study surface morphology of film samples of PVA/PANI/Ni nanoparticles synthesized by gamma radiation. Figure 5 shows the AFM image of the film surface indicating irregular shape and size of the films mainly attributed to the PANI structure as shown by the SEM images.

Figure 5. AFM image of PVA/PANI/Ni nanoparticles irradiated at low dose of 10 kGy for 18.2 wt% metal precursor concentration.

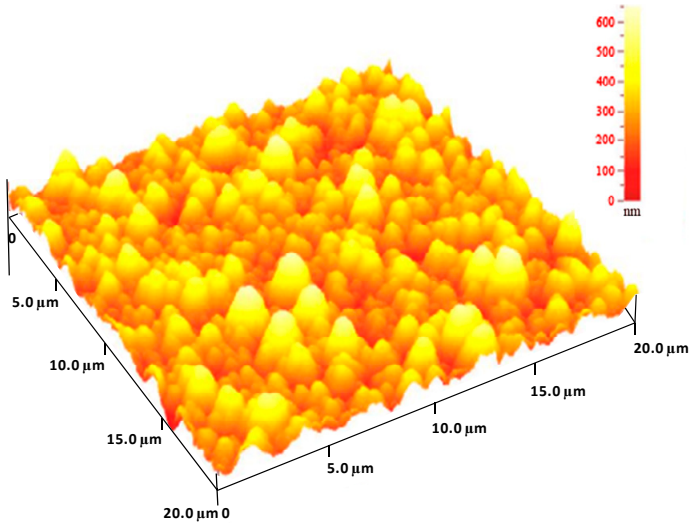

3.3. Optical Properties

Figure 6 shows the typical UV-visible absorption spectroscopy for PANI/Ni nanoparticles in PVA matrix films irradiated at different doses up to 50 kGy. The first sharper peak at around 390 nm is associated to the absorption peak of Ni nanoparticles, which blue-shifted from 395 to 381 nm with dose increasing from 0 to 50 kGy due to a decrease in nanoparticle size. Moreover, increasing the absorbed dose increased the absorbance of Ni nanoparticles because the concentration of Ni nanoparticles increases at higher doses. The second broader peak at around 720 nm is associated to the absorption peak of conducting PANI, which is partially oxidized. Increase the absorbed dose increased the absorbance of PANI due to increase of polarons formation, the electrical conducting agent of PANI.

Figure 6. UV-visible absorption spectra of PANI/Ni nanoparticles irradiated by different radiation doses for 18.2 wt% metal precursor concentration.

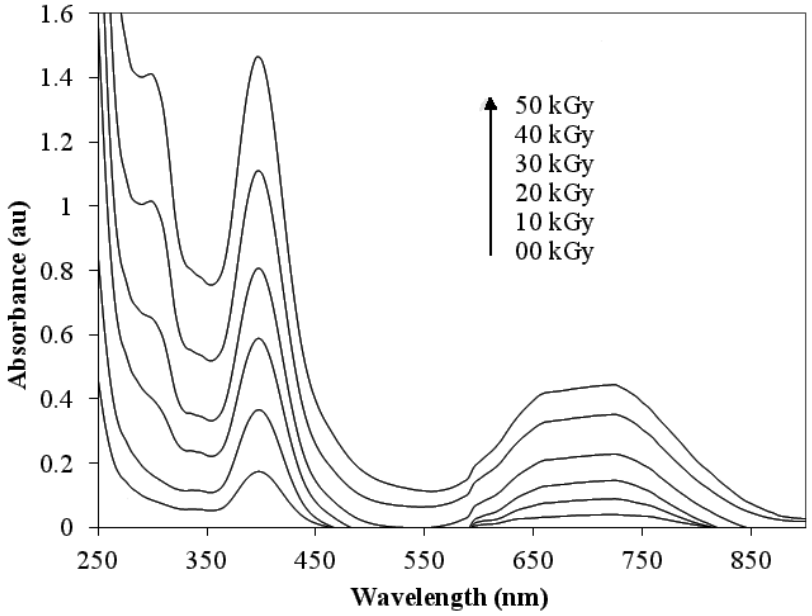

3.3.1. Conduction Band of Ni Nanoparticles

According the established theory of metal nanoparticles the absorption peak at around 390 nm (Figure 6) is due to Plasmon phenomenon in Ni nanoparticles. Gustav Mie in 1908 was first to introduce the theory of metal nanoparticles based on classical Maxwell equations of electrodynamics. The absorption phenomenon of metal nanoparticles is termed as a collective coherent oscillation of free conduction electrons with respect to the positive metallic lattice on the surface of metal–dielectric interface in resonance with the incoming electromagnetic fields. It is known as the localized surface Plasmon resonance (LSPR) with the scattering and absorption (or extinction) cross-sections are all strongly enhanced at resonance frequency. The cross section may be expressed in terms of the real and imaginary components of metal dielectric constants, the dielectric constant of the medium and the radius of the particle. However, a number of fundamental issues of metal nanoparticles cannot be addressed using the classical electromagnetic principle, such as quantum confinement effect of electrons and catalytic action of the metal nanoparticles.

Recently, optical absorption of metal nanoparticles based on quantum mechanics has been proposed [43,44] and confirmed experimentally [38,45]. In this theory of metal nanoparticles, the absorption of light can be described as a result of non-radiative intra-band excitations of conduction electrons from the lowest energy state assigned by the quantum numbers to higher energy states near the Fermi level of the conduction band. The electronic configuration of Ni nanoparticle takes the jellium shell model of electronic structure $Ni(28)_N$: $[Ar]_N$ $(4s^2)_N$ $(3d^8)_N$, where N is the number of atoms. The conduction electrons $(3d^8)_N$ are not absolutely free as in the Plasmon description, but weakly attach to the crystal backbone at the lowest energy state with the principle quantum number n (n = 3) and angular quantum number l (l = 2). The conduction electrons move around the positive metallic core and their energy may be described as a function of the conduction electrons density. The conduction band is the minimum energy of intra-band excitations of conduction electrons, $E = hc/\lambda_{max}$, where h is the Planck's constant, c is the speed of light, and λ_{max} is the wavelength of the absorption peak. The conduction band represents the energy required to free conduction electrons from the attraction of crystal backbone of Ni nanoparticles initiated by the electromagnetic UV-visible light. Figure 7 shows the conduction band increased linearity with increasing dose from 10 to 50 kGy at a given metal precursor concentration, which is attributed to a decrease in particle size.

Figure 7. Conduction band energy of Ni nanoparticles *versus* gamma dose for different metal precursor concentrations, the linear lines are drawn to fit the experimental data.

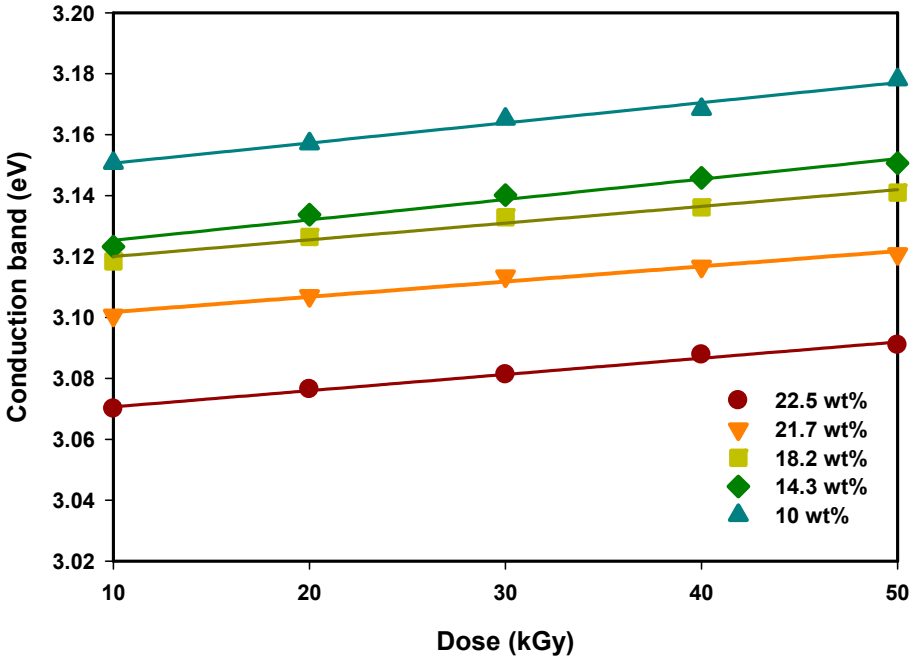

Figure 8 shows the conduction band of Ni nanoparticles decreased with increasing particle sizes for different precursor concentrations. For smaller particles, the number of atoms to make up a particle is few so that conduction electrons are less attracted to ionic core protons of the Ni nanoparticle and consequently increase the conduction band and decrease the absorption peak. As the concentration of the precursor decreased the conduction bands increase due to decrease of particle size. At low precursor concentration, in which the unreduced Ni^{2+} ions concentration is lower, more Ni^0 nucleation are formed by hydrated electrons and less $Ni^0{}_m$ nanoparticles ionized by $Ni^{2+}{}_n$ ions to form larger

$Ni^{2+}{}_{m+n}$ ions. Conversely, at high precursor concentration, in which the unreduced Ni^{2+} ions concentration is higher, more $Ni^{0}{}_{m}$ nanoparticles can be ionized by $Ni^{2+}{}_{n}$ ions to form larger $Ni^{2+}{}_{m+n}$ ions, and consequently into larger $Ni^{0}{}_{m+n}$ nanoparticles by hydrated electrons [38].

Figure 8. Conduction bands of Ni nanoparticles in PVA *versus* average size for different metal precursorconcentrations.

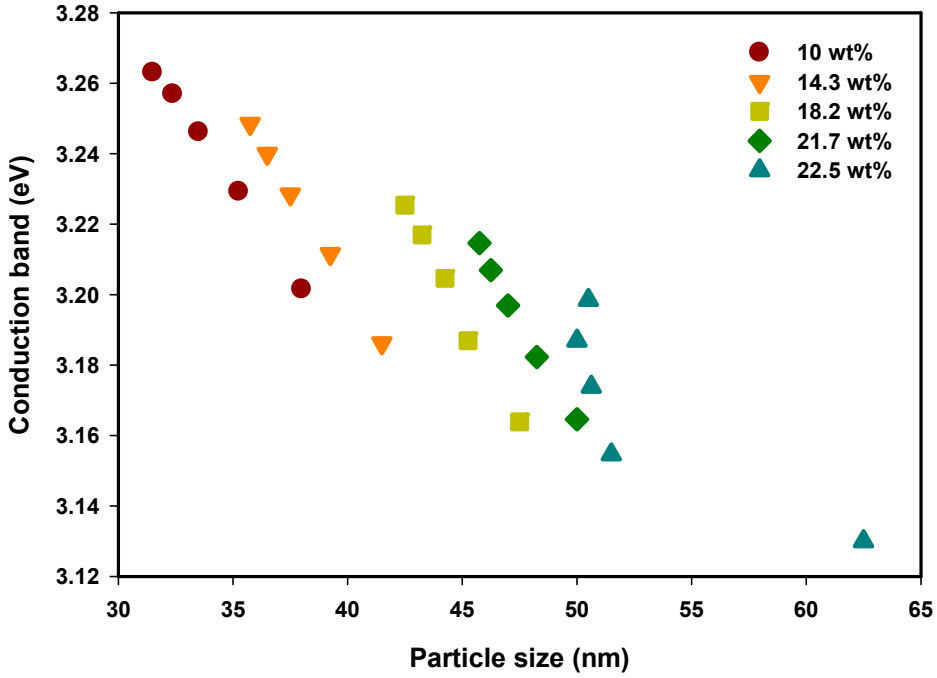

3.3.2. Band Gap of PANI

The optical absorption of PANI at 720 nm is associated with the electronic transitions from highly occupied molecular orbital (HOMO) π-band to lowly unoccupied molecular orbital (LUMO) π*-band of electronic states. The absorbance at ~720 nm band increases with increasing of dose, suggesting the oxidation or polymerization of PANI increases at higher doses (Figure 6). This result is in agreement with the result obtained for chemically synthesized PANI using HCl doping dispersed in PVA, having absorption bands between 740 and 800 nm [46]. The absorption coefficient α(ν) describes the absorption of photons along its track in a medium given as $\alpha(\nu) = 2.303A/d$, where d is distance into the medium in centimeter (cm). A, is the absorbance defined by $A = \log(I_0/I)$, where I_0 is the intensity of the incident beam and I is the intensity of transmitted beam. For $\alpha > 10^4$ cm^{-1}, the PANI band gap denotes the energy between HOMO and LUMO and can be determined from the absorption coefficient according to [47]:

$$\alpha(\nu)h\nu = B\left(h\nu - E_g\right)^m \quad (10)$$

where, $h\nu$ is the energy of the incidence photon, h is the Planck constant, E_g is the optical band gap energy, B is a constant known as the disorder parameter which is dependent on composition and independent to photon energy. Parameter m is the power coefficient with the value that is determined by the type of possible electronic transitions, *i.e.*, 1/2, 3/2, 2 or 1/3 for direct allowed, direct forbidden, indirect allowed and indirect forbidden respectively. The direct allowed band gap of PANI nanoparticles in different doses were evaluated from the plot of $(\alpha(\nu)h\nu)^2$ *versus* energy ($h\nu$) and by extrapolation

of the linear portions of curves to the energy axis for $(\alpha(\nu)h\nu)^2 = 0$. Figure 9 shows the band gap decreases with the increase of dose and precursor concentration because of increase of polarons with increasing dose and chlorine ions. The results show that when the doses were increased from 10 to 50 kGy the band gap decreases from 1.56 to 1.4 eV for 10 wt% of $NiCl_2$and from 1.54 to 1.33 eV for 22.5 wt% of $NiCl_2$.

Figure 9. Band gap (E_g) of PANI nanoparticles *versus* dose for different metal precursor concentrations. The exponentially lines indicate empirical equation which fitted through experimental data.

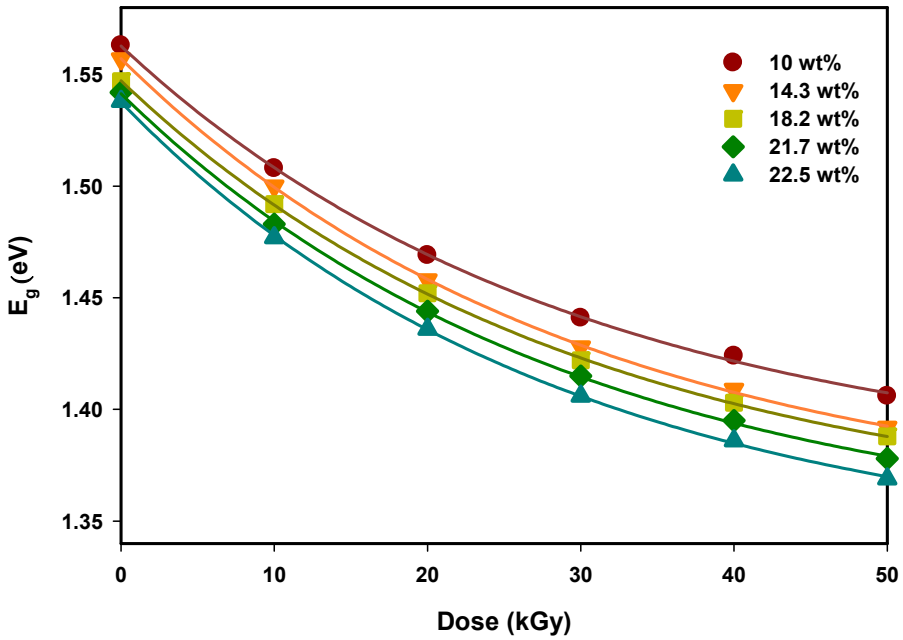

3.4. Electrical Conductivity

Figure 10 shows that the conductivity of the PVA/PANI/Ni nanoparticles film increases with the increase of radiation dose. The conductivity can be expressed according to [48]:

$$\sigma(\omega) = \sigma_{dc}(0) + \sigma_{ac}(\omega) \quad (11)$$

where $\sigma_{dc}(0)$ is the DC conductivity, $\sigma_{ac}(\omega)$ is the AC conductivity, and ω is the frequency. The DC conductivity of samples is mainly due to polarons of PANI and some free H^+, OH^- and Cl^- ions induced by γ radiation, which increases with increasing dose [49]. The AC conductivity is likely came from trapped polarons and ions such as H^+, OH^-, and Cl^- induced by radiation. The conductivity increases with the increase of dose and precursor concentration, corresponds with the increase of polarons amount. This has been confirmed from the previous optical study that the band gap energy of PANI decreases with the increase of dose and precursor concentration, indicating the increase of polarons in the samples.

Figure 10. Variation of total conductivity *versus* frequency of PANI/Ni nanoparticles in PVA films at different doses with 18.2 wt% metal precursor concentration.

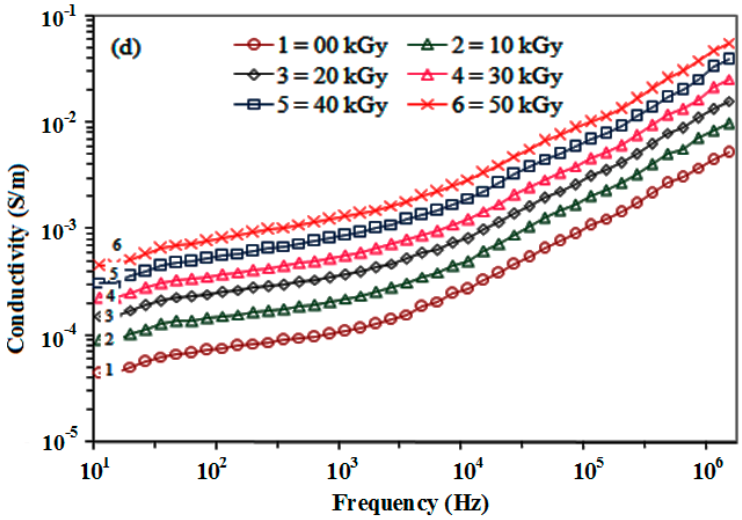

3.5. DC Conductivity of PVA/PANI/Ni Nanoparticle Films

Figure 11 shows the extrapolated DC conductivity $\sigma_{dc}(0)$ *versus* radiation dose for PVA/PANI/Ni nanoparticle films at different $NiCl_2$ concentrations. The DC conductivity increases with increasing dose and precursor concentration because more polarons are formed at higher doses and precursor concentrations. The result shows that when the doses were increased from 10 to 50 kGy the DC conductivity increases from 2.38×10^{-4} to 7.10×10^{-4} (S/m) for 10 wt% of $NiCl_2$ and from 5.98×10^{-3} to 3.48×10^{-2} (S/m) for 22.5 wt % of $NiCl_2$.

Figure 11. The DC conductivity *versus* dose for composites of PANI/Ni nanoparticles dispersed in PVA matrix films deduced by direct extrapolation.

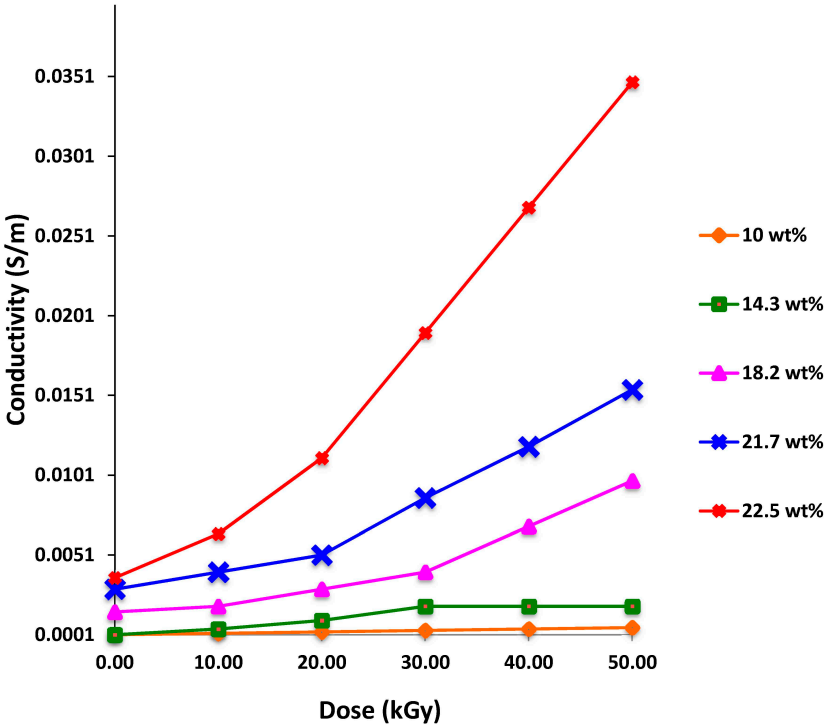

4. Conclusions

In summary, we have synthesized PANI/Ni nanocomposites dispersed in PVA matrix films by gamma radiolytic technique. The presence of Ni nanoparticles in PANI was confirmed by XRD, SEM and TEM analysis. The results show that the average particle size of Ni nanoparticles decreased with increasing dose and decreasing the precursor concentration due to increase of nucleation over aggregation process. Optical absorption spectra show a blue shift of the absorption peak of Ni nanoparticles due to decreasing particle size with increasing of dose. The optical band gap of PANI decreased with increasing of dose and chlorine concentration. Moreover, the absorbance of both PANI and Ni nanoparticles increased with dose due to increase of polarons and Ni nanoparticles formation. Finally, the electrical conductivity of the nanocomposites increased with the increase of dose and chlorine concentration corresponds to the increased amount of polarons.

Acknowledgments

This work was supported by the Ministry of Higher Education of Malaysia under the Fundamental Research and University Research grants. The authors would also like to thank the staff of the Faculty of Science and Bioscience Institute of the University Putra Malaysia, who contributed to this work.

Author Contributions

Abdo Mohd Meftah prepared the samples and organized the measurements, Elham Gharibshahi modeled and calculated the conduction bands, Nayereh Soltani edited the figures, W. Mahmooud Mat Yunus co-supervised the research, and Elias Saion supervised the research and wrote the manuscript.

Conflicts of Interest

The authors declare no conflict of interest.

References

1. Ali, M.A.; Saion, E.; Yahya, N.; Kassim, A.; Dahlan, K.M.; Hashim, S. Synthesis of conducting polyaniline nanocomposites by radiation doping. *J. Eng. Sci. Technol.* **2007**, *2*, 111–118.
2. Reda, S.M.; Al-Ghannam, S.M. Synthesis and electrical properties of polyaniline composite with silver nanoparticles. *Adv. Mater. Phys. Chem.* **2012**, *2*, 75–81.
3. Chuang, F.-Y.; Yang, S.-M. Cerium dioxide/polyaniline core–shell nanocomposites. *J. Colloid Interface Sci.* **2008**, *320*, 194–201.
4. Li, L.; Yan, G.; Wu, J.; Yu, X.; Guo, Q. Preparation of polyaniline–metal composite nanospheres by *in situ* microemulsion polymerization. *J. Colloid Interface Sci.* **2008**, *326*, 72–75.
5. Wankhede, Y.B.; Kondawar, S.B.; Thakare, S.R.; More, P.S. Synthesis and characterization of silver nanoparticles embedded in polyaniline nanocomposite. *Adv. Mater. Lett.* **2013**, *4*, doi:10.5185/amlett.2012.icnano.108.
6. Goto, H. A possibility for construction of an iodine cleaning system based on doping for π-conjugated polymers. *Polymers* **2011**, *3*, 875–885.

7. Stejskal, J.; Gilbert, R.G. Polyaniline: Preparation of a conducting polymer (IUPAC technical report). *Pure Appl. Chem.* **2002**, *74*, 857–867.
8. Bhadra, S.; Singha, N.K.; Khastgir, D. Electrochemical synthesis of polyaniline and its comparison with chemically synthesized polyaniline. *J. Appl. Polym. Sci.* **2007**, *104*, 1900–1904.
9. Khanna, P.K.; Singh, N.; Charan, S.; Viswanath, A.K. Synthesis of Ag/polyaniline nanocomposite via an *in situ* photo-redox mechanism. *Mater. Chem. Phys.* **2005**, *92*, 214–219.
10. Ali, M.; Saion, E.; Noorhana, Y.; Kassim, A.; Dahlan, K.; Rabaeh, K.; Shahrim, I.; Hashim, S. Chemical modification and control of polyaniline nanocomposites conductivity by radiation technique in PVA matrix. *J. Eng. Sci. Technol.* **2007**, *2*, 280–289.
11. Sridevi, V.; Malathi, S.; Devi, C. Synthesis and characterization of polyaniline/gold nanocomposites. *Chem. Sci. J.* **2011**, *2011*, 1–26.
12. Athawale, A.A.; Bhagwat, S. Synthesis and characterization of novel copper/polyaniline nanocomposite and application as a catalyst in the Wacker oxidation reaction. *J. Appl. Polym. Sci.* **2003**, *89*, 2412–2417.
13. Nabid, M.R.; Golbabaee, M.; Moghaddam, A.B.; Dinarvand, R.; Sedghi, R. Polyaniline/TiO_2 nanocomposite: Enzymatic synthesis and electrochemical properties. *Int. J. Electrochem. Sci.* **2008**, *3*, 1117–1126.
14. Houdayer, A.; Schneider, R.; Billaud, D.; Ghanbaja, J.; Lambert, J. New polyaniline/Ni(0) nanocomposites: Synthesis, characterization and evaluation of their catalytic activity in Heck couplings. *Synth. Met.* **2005**, *151*, 165–174.
15. Chen, D.-H.; Hsieh, C.-H. Synthesis of nickel nanoparticles in aqueous cationic surfactant solutions. *J. Mater.Chem.* **2002**, *12*, 2412–2415.
16. Chen, Y.; Peng, D.-L.; Lin, D.; Luo, X. Preparation and magnetic properties of nickel nanoparticles via the thermal decomposition of nickel organometallic precursor in alkylamines. *Nanotechnology* **2007**, *18*, doi:10.1088/0957-4484/18/50/505703.
17. Wang, A.; Yin, H.; Lu, H.; Xue, J.; Ren, M.; Jiang, T. Effect of organic modifiers on the structure of nickel nanoparticles and catalytic activity in the hydrogenation of *p*-nitrophenol to *p*-aminophenol. *Langmuir* **2009**, *25*, 12736–12741.
18. Kim, S.-G.; Terashi, Y.; Purwanto, A.; Okuyama, K. Synthesis and film deposition of Ni nanoparticles for base metal electrode applications. *Colloid Surf. A* **2009**, *337*, 96–101.
19. Hyeon, T. Chemical synthesis of magnetic nanoparticles. *Chem. Commun.* **2003**, *8*, 927–934.
20. Zhang, J.; Lan, C.Q. Nickel and cobalt nanoparticles produced by laser ablation of solids in organic solution. *Mater. Lett.* **2008**, *62*, 1521–1524.
21. Luo, X.; Chen, Y.; Yue, G.-H.; Peng, D.-L.; Luo, X. Preparation of hexagonal close-packed nickel nanoparticles via a thermal decomposition approach using nickel acetate tetrahydrate as a precursor. *J. Alloy. Compd.* **2009**, *476*, 864–868.
22. Davar, F.; Fereshteh, Z.; Salavati-Niasari, M. Nanoparticles Ni and NiO: Synthesis, characterization and magnetic properties. *J. Alloy. Compd.* **2009**, *476*, 797–801.
23. Xu, W.; Liew, K.Y.; Liu, H.; Huang, T.; Sun, C.; Zhao, Y. Microwave-assisted synthesis of nickel nanoparticles. *Mater. Lett.* **2008**, *62*, 2571–2573.

24. Couto, G.G.; Klein, J.J.; Schreiner, W.H.; Mosca, D.H.; de Oliveira, A.J.; Zarbin, A.J. Nickel nanoparticles obtained by a modified polyol process: Synthesis, characterization, and magnetic properties. *J. Colloid Interface Sci.* **2007**, *311*, 461–468.
25. Wang, W.-N.; Itoh, Y.; Lenggoro, I.W.; Okuyama, K. Nickel and nickel oxide nanoparticles prepared from nickel nitrate hexahydrate by a low pressure spray pyrolysis. *Mater. Sci. Eng. B* **2004**, *111*, 69–76.
26. Kauffeldt, E.; Kauffeldt, T. Thermodynamic-controlled gas phase process for the synthesis of nickel nanoparticles of adjustable size and morphology. *J. Nanopart. Res.* **2006**, *8*, 477–488.
27. Beach, E.R.; Shqau, K.; Brown, S.E.; Rozeveld, S.J.; Morris, P.A. Solvothermal synthesis of crystalline nickel oxide nanoparticles. *Mater. Chem. Phys.* **2009**, *115*, 371–377.
28. Aslani, A.; Oroojpour, V.; Fallahi, M. Sonochemical synthesis, size controlling and gas sensing properties of NiO nanoparticles. *Appl. Surf. Sci.* **2011**, *257*, 4056–4061.
29. Chen, D.-H.; Wu, S.-H. Synthesis of nickel nanoparticles in water-in-oil microemulsions. *Chem. Mater.* **2000**, *12*, 1354–1360.
30. Liu, R.; Qiu, H.; Li, H.; Zong, H.; Fang, C. Fabrication and characteristics of composite containing HCl-doped polyaniline and Ni nanoparticles. *Synth. Met.* **2010**, *160*, 2404–2408.
31. Uygun, A.; Aslan, E. Comparative study of conducting polyaniline/copper and polyaniline/nickel composites in the presence of surfactants. *Polym. Int.* **2010**, *59*, 1162–1167.
32. Trung, T.; Trung, T.H.; Ha, C.-S. Preparation and cyclic voltammetry studies on nickel-nanoclusters containing polyaniline composites having layer-by-layer structures. *Electrochim. Acta* **2005**, *51*, 984–990.
33. Dalla Corte, D.A.; Torres, C.; Correa, P.D.S.; Rieder, E.S.; Malfatti, C.D.F. The hydrogen evolution reaction on nickel-polyaniline composite electrodes. *Int. J. Hydrog. Energy* **2012**, *37*, 3025–3032.
34. Naghavi, K.; Saion, E.; Rezaee, K.; Yunus, W.M.M. Influence of dose on particle size of colloidal silver nanoparticles synthesized by gamma radiation. *Radiat. Phys. Chem.* **2010**, *79*, 1203–1208.
35. Wu, S.-H.; Chen, D.-H. Synthesis and characterization of nickel nanoparticles by hydrazine reduction in ethylene glycol. *J. Colloid Surface Sci.* **2003**, *259*, 282–286.
36. Kharazmi, A.; Saion, E.; Faraji, N.; Soltani, N.; Dehzangi, A. Optical properties of CdS/PVA nanocomposite films synthesized using the gamma-irradiation-induced method. *Chin. Phys. Lett.* **2013**, *30*, doi:10.1088/0256-307X/30/5/057803.
37. Soltani, N.; Saion, E.; Hussein, M.Z.; Erfani, M.; Rezaee, K.; Bahmanrokh, G. Phase controlled monodispersed CdS nanocrystals synthesized in polymer solution using microwave irradiation. *J. Inorg. Organomet. Polym. Mater.* **2012**, *22*, 830–836.
38. Gharibshahi, E.; Saion, E. Influence of dose on particle size and optical properties of colloidal platinum nanoparticles. *Int. J. Mol. Sci.* **2012**, *13*, 14723–14741.
39. Zhao, H.T..; Han, X.J.; Zhang, L.F.; Wang, G.Y.; Wang, C.; Li, X.A.; Xu, P. Controlled synthesis and morphology-dependent electromagnetic properties of nickel nanostructures by γ-ray irradiation technique. *Radiat. Phys. Chem.* **2011**, *80*, 390–393.
40. Yang, C.; Chen, C. Synthesis, characterisation and properties of polyanilines containing transition metal ions. *Synth. Met.* **2005**, *153*, 133–136.

41. Cho, M.S.; Park, S.Y.; Hwang, J.Y.; Choi, H.J. Synthesis and electrical properties of polymer composites with polyaniline nanoparticles. *Mater. Sci. Eng. C* **2004**, *24*, 15–18.
42. Dispenza, C.; Presti, C.L.; Belfiore, C.; Spadaro, G.; Piazza, S. Electrically conductive hydrogel composites made of polyaniline nanoparticles and poly (*N*-vinyl-2-pyrrolidone). *Polymer* **2006**, *47*, 961–971.
43. Gharibshahi, E.; Saion, E. Quantum mechanical calculation of optical absorption of silver and gold nanoparticles by density functional theory. *Phys. Int.* **2010**, *1*, 57–64.
44. Saion, E.; Gharibshahi, E. On the theory of metal nanoparticles based on quantum mechanical calculation. *J. Fund. Sci.* **2011**, *7*, 6–11.
45. Saion, E.; Gharibshahi, E.; Naghavi, K. Size-controlled and optical properties of monodispersed silver nanoparticles synthesized by the radiolytic reduction method. *Int. J. Mol. Sci.* **2013**, *14*, 7880–7896.
46. Malmonge, J.; Mattoso, L. Doping of polyaniline and derivatives induced by X-ray radiation. *Synth. Met.* **1997**, *84*, 779–780.
47. Soltani, N.; Gharibshahi, E.; Saion, E. Band gap of cubic and hexagonal CdS quantum dots-experimental and theoritical studies. *Chalcogenide Lett.* **2012**, *9*, 321–328.
48. Dutta, P.; Biswas, S.; Ghosh, M.; De, S.; Chatterjee, S. The DC and AC conductivity of polyaniline–polyvinyl alcohol blends. *Synth. Met.* **2001**, *122*, 455–461.
49. De Oliveira, Z.; dos Santos, M. Relative stability of polarons and bipolarons in emeraldine oligomers: A quantum chemical study. *Solid State Commun.* **2000**, *114*, 49–53.